Cornea

Differential Distribution of Laminin N-Terminus α31 Across the Ocular Surface: Implications for Corneal Wound Repair

Valentina Barrera, Lee D. Troughton, Valentina Iorio, Siyin Liu, Olutobi Oyewole, Carl M. Sheridan, and Kevin J. Hamill

Department of Eye and Vision Science, Institute of Ageing and Chronic Disease, University of Liverpool, Liverpool, United Kingdom

Correspondence: Kevin J. Hamill, Department of Eye and Vision Science, Institute of Ageing and Chronic Disease, William Henry Duncan Building, University of Liverpool, L7 8TX, 6 West Derby Street, Liverpool, UK;
khamill@liverpool.ac.uk.

VB and LDT contributed equally to the work presented here and should therefore be regarded as equivalent authors.

PURPOSE. Laminin N-terminus (LaNt) α31 is a relatively unstudied protein derived from the laminin α3 gene but structurally similar to netrins. LaNt α31 has, to date, been investigated only in two-dimensional (2D) keratinocyte culture where it influences cell migration and adhesion, processes integral to wound repair. Here we investigated LaNt α31 distribution in ocular surface epithelium, during limbal stem cell activation, and corneal wound healing.

METHODS. Human, mouse, and pig eyes, ex vivo limbal explant cultures, and alkali burn wounds were processed for immunohistochemistry with antibodies against LaNt α31 along with progenitor cell–associated proteins. LaNt α31 expression was induced via adenoviral transduction into primary epithelial cells isolated from limbal explants, and cell spreading and migration were analyzed using live imaging.

RESULTS. LaNt α31 localized to the basal layer of the conjunctival, limbal, and corneal epithelial cells. However, staining was nonuniform with apparent subpopulation enrichment, and some suprabasal reactivity was also noted. This LaNt α31 distribution largely matched that of keratin 15, epidermal growth factor receptor, and transformation-related protein 63α (p63α), and displayed similar increases in expression in activated limbal explants. During active alkali burn wound repair, LaNt α31 displayed increased expression in limbal regions and loss of basal restriction within the cornea. Distribution returned to predominately basal cell restricted once the wounded epithelium matured. Cultured corneal epithelial cells expressing LaNt α31 displayed increased 2D area and reduced migration, suggesting a functional link between this protein and key wound repair activities.

CONCLUSIONS. These data place LaNt α31 in position to influence laminin-dependent processes including wound repair and stem cell activation.

Keywords: cornea, ocular surface epithelium, corneal wound healing, basement membrane, laminin

Laminin N-terminus (LaNt) α31 is member of a relatively unstudied family of proteins generated by alternative splicing from laminin-encoding genes. To date, only one study describing LaNt function has been published, which suggested a role for LaNt α31 in the regulation of epidermal keratinocyte adhesion and migration, likely through influencing laminins.[1] These data suggest that LaNt α31 could influence tissue remodeling. Therefore, knowledge of this protein's distribution in healthy tissue and in disease contexts, such as during corneal repair, is key to understanding when and where it could exert its effects. In this study, we have focused on the ocular surface epithelium, where laminins are key mediators of numerous processes including regulating limbal stem cell maintenance and corneal repair processes.[2–7]

Laminins contribute to a wide variety of cellular behaviors; however, they are best understood for their structural roles as core components of specialized regions of extracellular matrix, termed basement membranes (BM). BM underlie and support all epithelial and endothelial sheets of cells as well as nerves and muscles (for reviews see Refs. 8–10). In addition to their structural support roles, laminins also present cell surface receptor binding sites and initiate a variety of outside-in signaling cascades. Many of these are context specific, including regulating proliferation and adhesion and influencing the ability of cells to generate the traction forces required for migration.[8–10] Moreover, there is increasing evidence that specific laminins can contribute to either maintaining stem cells in an undifferentiated state, or can help drive cells down a defined differentiation pathway depending on which of the 16 different laminin family members the cells interact with.[11–18]

LaNt α31 is generated from the *LAMA3* gene, which encodes two laminin subunits; α3a and α3b.[1,19,20] Laminin α3b has not been as extensively investigated; however, laminin α3a is highly expressed in the ocular surface epithelium where it is directly implicated in conjunctival, limbal, and corneal epithelial cell function, and dysfunction is associated with a variety of ocular pathologies.[3,5,7] Specifically, laminin α3 has been shown to be critical for epithelial integrity, demonstrated by the inherited disease junctional epidermolysis bullosa where patients with mutations in *LAMA3* present with widespread epithelial fragility including effects on the corneal epithelium.[21,22] Similarly, in the autoimmune disorder mucous membrane

4082

Investigative Ophthalmology & Visual Science

pemphigoid, a subset of patients present with circulating autoantibodies against laminin α3, which leads to blistering and scarring.[23-25] Patients with mutations specific to the laminin α3a isoform develop laryngo-onycho-cutaneous syndrome, which manifests in the eye as chronic overproduction of granulation tissue, suggesting a role for this laminin in controlling scarring.[26] Moreover, laminin α3 as part of laminin α3β3γ2 (LM332, formerly laminin 5) provides the substrate for cell migration during wound repair, and defective clearance of damaged BM, including laminin α3, leads to recurrent erosions in a condition termed map dot fingerprint syndrome.[6,27,28] More generally, changes to laminin expression levels are also associated with keratoconus, diabetes, and ageing.[4,29,30]

Although derived from a laminin gene, LaNt α31 is much smaller than laminin subunits and does not contain many of the domains responsible for laminin functions.[8] Most notably, LaNts contain neither the archetypal laminin coiled-coil domain, through which heterotrimerization occurs, nor the carboxyl terminal laminin globular domains, which harbor the highest-affinity integrin binding sites.[31-35] In contrast, in LaNt α31 the main structural feature is a laminin N-terminal (LN) domain, which is the domain through which laminin-to-laminin interactions and therefore laminin network assembly occur.[36-38] The LaNt α31 LN domain is followed by a short stretch of laminin-type epidermal growth factor-like repeats (LE domains) and a short unique C-terminus with no known conserved domain homology.[1] The structure of a LN domain followed by LE repeats is shared by a second family of extracellular matrix proteins, the netrins. Netrins are best known for their roles in axonal guidance; however, netrin-4 has also been shown to influence laminin network assembly.[39,40] Specifically in the front of the eye, netrins-1 and -4 have been implicated in wound repair, inflammation, and angiogenesis.[41-44]

At the protein level, LaNt α31 has previously been shown to be expressed in the skin; however, widespread expression at the transcript level in other tissues has also been described.[1] The ocular surface epithelium shows more definitive local specificity than the epidermis in terms of function and BM composition. Specifically, the surface epithelium can be considered as three distinct regions: the conjunctiva, which provides a mucous (tear film)-producing epithelium; the corneal–limbal region, which provides an epithelial stem cell niche; and the central corneal epithelium, which provides a transparent barrier layer. All three of these regions have LAMA3 promoter activity and are therefore good candidates to also express LaNt α31.[2,3,5,7,45] In this study, we have investigated LaNt α31 expression across the ocular surface epithelia in human, mouse, and pig eyes, in intact tissue, and in ex vivo conditions designed to mimic stem cell activation and epithelial wound repair. The impact of LaNt α31 on cell functions was directly investigated by isolating human primary corneal epithelial cells from limbal explants and inducing expression of LaNt α31.

METHODS

Ethical Approval

Research with human subjects followed the tenets of the Declaration of Helsinki. All experiments on human tissues were approved by the University of Liverpool and UK National Health Service Health Research Authority ethics committees (#16/EM/0090, #T0093). Specific informed consent from donor or family members was acquired before human corneal limbal rim use. All animal procedures adhered to the ARVO Statement for the Use of Animals in Ophthalmic and Vision Research.

Antibodies

Rabbit polyclonal antibodies against human LaNt α31 were described previously.[1] Rabbit polyclonal antibodies against keratin 12[46] and LM332,[47] and mouse monoclonal antibodies against laminin α3 (RG13),[48] were kind gifts from Jonathan Jones, Washington State University, Washington, United States. Rabbit polyclonal antibodies against epidermal growth factor receptor (EGFR; 1:100, #06-847; Merck Millipore, Darmstadt, Germany), transformation-related protein 63α (p63α; 1:250, #4892S; Cell Signaling Technology, Danvers, MA, USA), cytokeratin 5 (K5, 1:100 ab53121; Abcam, Cambridge, MA, USA), and mouse monoclonal antibodies against cytokeratin 15 (K15, 1:500, ab80522; Abcam) and vimentin (clone V9, 1:100; Sigma-Aldrich, Poole, UK) were used for immunohistochemistry and/or immunofluorescence microscopy. Rabbit (1:200) and mouse (1:1000) IgG controls were obtained from BD Biosciences (San Jose, CA, USA). Anti-mouse and anti-rabbit secondary antibodies for immunohistochemistry were obtained from EnVision + System-HRP kit (ready-to-use solution; Agilent, Santa Clara, CA, USA). Cy5 and fluorescein isothiocyanate–conjugated goat anti-mouse IgG and tetramethylrhodamine-conjugated goat anti-rabbit IgG were obtained from Jackson Labs (Sacramento, CA, USA). Goat anti-mouse IRDye 800CW and goat anti-rabbit IRDye 680CW were obtained from LiCor BioSciences (Rugby, UK).

Mouse monoclonal antibodies against human LaNt α31 (clone 3E11) were raised against a synthetic peptide corresponding to residues 437 to 451 (VLPQRSHQANFGSV; GenWay Biotech, San Diego, CA, USA) conjugated to keyhole limpet hemocyanin following the procedure previously described[47] with help from the recombinant protein production core at Northwestern University (Chicago, IL, USA). Five days following the final boost, the spleen was removed and isolated splenocytes were fused with the myeloma cell line Sp2 for the production of hybridomas.[49] Hybridoma clones were selected on the basis of ELISA reactivity to the unconjugated peptide and then tested for immunoblotting reactivity against a human epidermal keratinocyte (HaCaT[50]) protein extract. Selected hybridoma cells were cloned twice by limited cell dilution. The final antibodies were used for immunohistochemistry and Western blotting at 1.6 μg/mL final concentration, and immunofluorescence microscopy at 5 μg/mL.

Rabbit polyclonal antibodies were raised against CLNSDSSMFSLSPRML (Eurogentec, Liège, Belgium) corresponding to mouse LaNt α31 residues 465 to 480. Antibodies were screened by ELISA against the unconjugated peptide, then by Western blotting against total protein extracts from mouse keratinocytes, and then affinity purified using the unconjugated peptide. Antigen depletion was performed by preincubating the anti-mouse LaNt α31 antibodies with the antigenic peptide (1 μM in 15 mM Na_2CO_3 35 mM $NaHCO_3$) overnight at 4°C.

Tissue Processing: Immunohistochemistry

Human donor eyes obtained from the Liverpool Research Eye Bank (Liverpool, UK) were sectioned anterior-posteriorly through the pupil and the anterior segment was analyzed separately. Mouse globes from 21-week-old B6CBAF1 female mice were processed as whole globes. In each case, tissues were fixed in 10% neutral buffered formalin (Leica, Wokingham, UK) for 24 hours at the time of dissection, then processed through graded ethanol and xylene before being embedded in paraffin wax.

Sections (4 μm) were cut using a rotary microtome RM2235 (Leica), adhered to microscope slides (EnVision FLEX system, Agilent), and then dried overnight at 37°C. Sections were then dewaxed and rehydrated through a series of decreasing ethanol concentrations. Antigen retrieval was performed by microwaving sections in preheated 0.01 M citrate buffer pH6 (Sigma-Aldrich) for 5 minutes. Endogenous peroxidases were blocked by treatment with 0.3% vol/vol hydrogen peroxide (15 minutes; Agilent), and then slides were blocked in 20% vol/vol goat serum (Sigma-Aldrich). Sections were then incubated with primary antibodies or isotype-matched controls at 4°C overnight (except for anti-EGFR, which was incubated at room temperature [RT] for 1 hour), followed by HRP-conjugated secondary antibodies at RT for 30 minutes (EnVision + System-HRP, Agilent). At each stage washing was performed with PBS with 0.1% Tween 20 (Sigma-Aldrich). HRP signal was detected using either 3,3′-diaminobenzidine (DAB, Agilent) or 3-amino-9-ethylcarbazole (AEC) chromogens at RT for 5 minutes. Sections were counterstained with filtered Mayer's hematoxylin (Leica), dehydrated through a series of ascending ethanol concentrations, and then mounted using either Pertex (HistoLab, Gothenburg, Sweden) for DAB or Aquatex mounting media (Merck Millipore) for AEC. Images were captured with an Olympus BX60 system microscope equipped with an Olympus DP71 digital camera and cell imaging software (Olympus, Southend-on-Sea, UK).

Scoring of immunohistochemistry staining, to evaluate LaNt α31 basal versus suprabasal expression, was performed by four independent observers analyzing red-green-blue (RGB) images following color deconvolution to remove hematoxylin signal using Fiji32 software (National Institutes of Health, Bethesda, MD, USA). A score of 0, 1, 2, or 3 was given to DAB-stained basal or suprabasal cells by each observer. Independent scorers had the full panel of stained sections available.

Tissue Processing: Immunofluorescence

Porcine anterior segments were snap frozen in liquid nitrogen before submerging in optimal cutting temperature compound (OCT) and freezing on dry ice. Human limbal rims were submerged in OCT and fast frozen on a dry ice/isopentane slurry. Tissue sections (5 μm), cut using Leica cryostat, were fixed in ice-cold acetone (Sigma-Aldrich) for 10 minutes, then incubated overnight at 4°C with primary antibodies or isotype-matched controls diluted in PBS with 5% vol/vol goat serum. Slides were washed in PBS, then incubated with secondary antibodies in PBS for 1 hour at 37°C. Slides were finally washed, then mounted in Vectashield mounting media containing 4′,6-diamidino-2-phenylindole (DAPI) (Vector Labs, Burlingame, CA, USA), and imaged using a Zeiss LSM800 confocal microscope (Zeiss, Jena, Germany).

Limbal Explant Culture

Human corneal limbal rims ($n = 10$), acquired from the Tissue and Eye Services at St. Pauls Eye Unit, Royal Liverpool University Hospital, Liverpool, were isolated from the remnants of donor corneas that had been used for penetrating keratoplasty. Excess scleral, iris tissue, and corneal endothelium were carefully removed from the corneal limbal rings, leaving a ring of approximately 3-mm diameter. The rings were dissected into ~2-mm cuboidal segments for ex vivo culture. These segments were placed in the center of a well of a 12-well culture plate (Corning, Inc., Corning, NY, USA) and cultured at 37°C and 5% CO_2 in limbal epithelial stem cell medium consisting of equal volumes of Dulbecco's modified Eagle's medium (DMEM) and Ham's F12 medium, 100 U/mL penicillin, 100 μg/mL streptomycin, and 2.5 μg/mL amphotericin B1 (all

Sigma-Aldrich), and 0.4 mg/mL hydrocortisone, 10 mg/mL insulin, 20 μg/mL tri-iodothyronine, 40 mg/mL adenine, 50 μg/mL cholera toxin, and 100 ng/mL epidermal growth factor (Lonza, Slough, UK). Medium was changed every 2 days and epithelial outgrowth monitored daily for 7 to 14 days with a phase-contrast microscope (Nikon, Surrey, UK); then explants displaying outgrowths were fixed and processed for immuno-histochemistry, or embedded in OCT and frozen for immuno-fluorescence processing.

Pig Corneal Wound Model

Porcine eyes were obtained from local abattoirs, and anterior segments were dissected by coronal incision within 6 hours of enucleation. Extraocular tissue, iris, ciliary body, and lens were removed, leaving only intact cornea and trabecular meshwork. Corneas were washed in PBS with 200 U/mL penicillin, 200 μg/mL streptomycin, and 5 μg/mL amphotericin B1. An alkali burn epithelial wound was induced as previously described[51] by using a sterile 5-mm-diameter round filter paper soaked in 0.5 M NaOH applied for 20 seconds to the central cornea. Tissues were maintained in culture for up to 72 hours following wounding, in high-glucose DMEM medium, supplemented with 10% fetal calf serum (FCS; Labtech East Sussex, UK), 2 mM L-glutamine, 100 U/mL penicillin, 100 μg/mL streptomycin, and 2.5 μg/mL amphotericin B on a rotary incubator, then washed, fixed, and processed for immunohis-tochemistry.

Cell Culture

Primary corneal epithelial cells (pCEC) were isolated from limbal explants after 14 days of ex vivo culture, by TrypLE Express Enzyme (Thermo Fisher Scientific, Waltham MA, USA), then cultured in limbal epithelial culture media. Spontaneously transformed human epidermal keratinocytes HaCaT[52] were cultured using DMEM (Sigma-Aldrich) supplemented with 10% FCS (LabTech) and 4 mM L-glutamine (Sigma-Aldrich).

Adenovirus Production and Cell Transduction

Full-length *LAMA3LN1* was PCR amplified from cDNA generated from cultured human keratinocytes, then cloned into pCR2.1 (Life Technologies, Carlsbad, CA, USA) and sequence verified by DNA sequencing (DNA Sequencing and Services, University of Dundee). The native translational stop codon was converted to an *Age*I restriction enzyme site by site-directed mutagenesis following the manufacturer's directions for QuikChange II XL mutagenesis kit (Agilent). The mutated *LAMA3LN1* was then subcloned using *Kpn*I and *Age*I (New England Biolabs, Hitchin, UK) into pENTR4 (Life Technologies) with eGFP inserted into the *Bgl*II and *Kpn*I sites of the multiple cloning site (a kind gift from Jonathan Jones, Washington State University, WA, USA). LR recombination was used to transfer the *LAMA3LN1-eGFP* construct from pENTR to pAD-CMV/V5-DEST (Life Technologies) and adenoviral particles produced following the standard gateway-adapted ViralPower adenoviral expression protocol (Life Technologies).

For cell transduction, 3×10^5 pCEC were seeded in 60-mm dishes (Greiner Bio-One, Stonehouse, UK), then transduced with adenovirus in 4 mL media 24 hours after seeding. Analyses of LaNt α31-GFP (+LaNt α31), GFP (+GFP), or untreated cells were conducted 48 to 72 hours following transduction.

Cell Migration and Cell Morphology Analyses

For cell morphology analyses and low-density migration assays, cells were seeded at 2.5×10^4 cells/well onto uncoated 24-well

plates (Greiner Bio-One). For morphology, ×20 phase-contrast images were acquired on a Nikon TiE microscope (Nikon), and cell perimeters of individual cells were manually traced to define cell area using Fiji32 software. For low-density migration assays, cells were imaged every 2 minutes over a 2-hour period, using a ×20 objective on a Nikon TiE fluorescent microscope; then individual cells were tracked using the MTrackJ plugin of the Fiji32.

Immunocytochemistry

Cells (1×10^5) were seeded for 5 hours on uncoated glass coverslips, then fixed and extracted in ice-cold ethanol for 4 minutes and air-dried. Primary antibodies were diluted in PBS with 20% normal goat serum (Jackson Labs) and incubated at 37°C for 2 hours; coverslips were then washed extensively with PBS prior to probing for 1 hour at 37°C with Cy5-conjugated secondary antibodies diluted 1:400 in PBS. Coverslips were washed in PBS 0.05% Tween 20, then mounted with polyvinyl alcohol mounting medium with DABCO (Sigma-Aldrich). Images were obtained using Zeiss LSM510 confocal microscope (Zeiss, Cambridge, UK).

RNA Isolation

Paired donor anterior segments after Descemet's stripping endothelial keratoplasty (DSEK) were dissected for either central or peripheral cornea RNA isolation. The trabecular meshwork and any residual iris tissue were removed from both eyes. The ocular surface epithelium from one anterior segment was removed by scraping with a scalpel blade to generate a stroma-only sample. The central cornea region (with or without epithelium) was then excised using a 5-mm trephine, and microscissors were used to isolate the peripheral corneal tissue containing the limbus and small amounts of conjunctiva and peripheral cornea. The extracted tissue was snap-frozen in liquid nitrogen and ground with a pestle and mortar before dissolving in 1 mL TRI reagent (Sigma-Aldrich) and freezing on dry ice. The samples were then thawed before adding 200 μL chloroform (Sigma-Aldrich), mixed thoroughly, and then incubated for 5 minutes at RT. The samples were centrifuged at 4°C for 15 minutes at 12,000g to separate phases. The upper RNA-containing phase was then added to the genomic DNA (gDNA) removal column from the Monarch Total RNA Miniprep Kit (New England Biolabs), and the manufacturer's protocol was followed to isolate total RNA.

RNA from pCEC was extracted using the Monarch Total RNA Miniprep Kit (New England Biolabs). Briefly, 200 μL lysis buffer was added directly to the cells following removal of explanted tissue. The cells were homogenized using a cell scraper, and the lysate was collected in a microcentrifuge tube before adding equal volume of absolute ethanol (Sigma-Aldrich) to precipitate the RNA following the manufacturer's protocol to isolate total RNA. RNA quality and quantity were measured using the Agilent TapeStation 2200, with a RNA integrity number of >8 deemed acceptable for further downstream analyses.

Reverse Transcription–Polymerase Chain Reaction

Following RNA extractions, 40 ng total RNA was reverse transcribed (RT) using Precision nanoScript 2 Reverse Transcription kit (Primerdesign, Southampton, UK), using a combination of oligo-dt and random hexamers. Intron-spanning primer pairs (Supplementary Table S1) were designed to amplify specific *LAMA3* isoform mRNAs, *GAPDH*, and *RPLO*, with primers being synthesized by Sigma-Aldrich. Isoform-specific PCR was performed using RedTaq PCR Readymix

(Sigma-Aldrich). RT-RNA (10 ng) was used in each reaction, with the following protocol: one cycle of 94°C for 5 minutes, 40 cycles of 94°C for 30 seconds, 60°C for 15 seconds, and 72°C for 30 seconds, followed by a final cycle of 72°C for 5 minutes. Then products were run on a 2% agarose gel with a 100–base pair ladder (Sigma-Aldrich). PCR products were sequence validated to confirm specificity (DNA Sequencing and Services).

RESULTS

LaNt α31 Displays Differential Expression Across the Human Ocular Surface Epithelium

LaNt α31 is produced from the same gene as laminin α3, which is well characterized as being abundantly expressed in conjunctival, limbal, and corneal epithelium.[5,7] To confirm expression at the transcript level, we performed isoform-specific RT-PCR using RNA extracted from human donor tissue donated after DSEK surgery, comparing expression in the central and peripheral cornea either with or without ocular surface epithelium (Supplementary Fig. S1). This confirmed the presence of *LAMA3LN1* mRNA in both the central and peripheral cornea and corneal stroma (Supplementary Fig. S1A).

Having confirmed expression at the mRNA level, we next investigated LaNt α31 protein distribution in human ocular anterior segments from postmortem tissue ($N = 10$) using two different antibodies raised against the human form of the protein. First, we used previously characterized rabbit poly-clonal antibodies raised against GST fusion protein of the entirety of the unique 54 amino acids of LaNt α31.[1] Secondly, we raised mouse monoclonal antibodies against a 14-mer peptide within the unique region of the protein. Hybridoma clones were screened by ELISA against the unconjugated peptide, then by Western blotting against protein extracts from HaCaT immortalized epidermal keratinocytes, and subsequently against protein extracts from cells expressing a LaNt α31-GFP fusion protein (Supplementary Figs. S1B, S1C). Both antibodies recognize the same products; however, compared with the rabbit pAb, the new anti-LaNt α31 mAb gave cleaner, more consistent staining (Supplementary Figs. S1B, S1C). Processing of limbal explants with both of these antibody preparations yielded near-identical distribution patterns, providing further validation for their shared specificity (Fig 1A; Supplementary Fig. S1D).

Immunohistochemistry staining revealed LaNt α31 expression in most cells of the basal layer of the conjunctival, corneal, and limbal epithelia, with higher overall staining observed within limbal regions (Fig. 1A; Supplementary Figs. S2, S3). Interestingly, the staining intensities were not uniform within each of the surface epithelial regions, with notable groups of cells displaying relatively higher expression compared with their neighbors (Fig. 1A; Supplementary Figs. S2, S3). We also observed suprabasal staining in addition to the expected basal localization of this protein; the frequency and relative intensity of this suprabasal staining varied between different donor eyes (Supplementary Table S2). Across the study population, conjunctival and limbal epithelium displayed similar general trends, with strong basal LaNt α31 staining and generally weak or absent staining in suprabasal cells (Supplementary Fig. S3; Supplementary Table S2). In the peripheral and central cornea, strong basal staining was observed in all samples. However, staining of suprabasal cells was more frequently present; indeed, more samples lacked the clear demarcation between basal and suprabasal staining intensities (7 of 10 cases
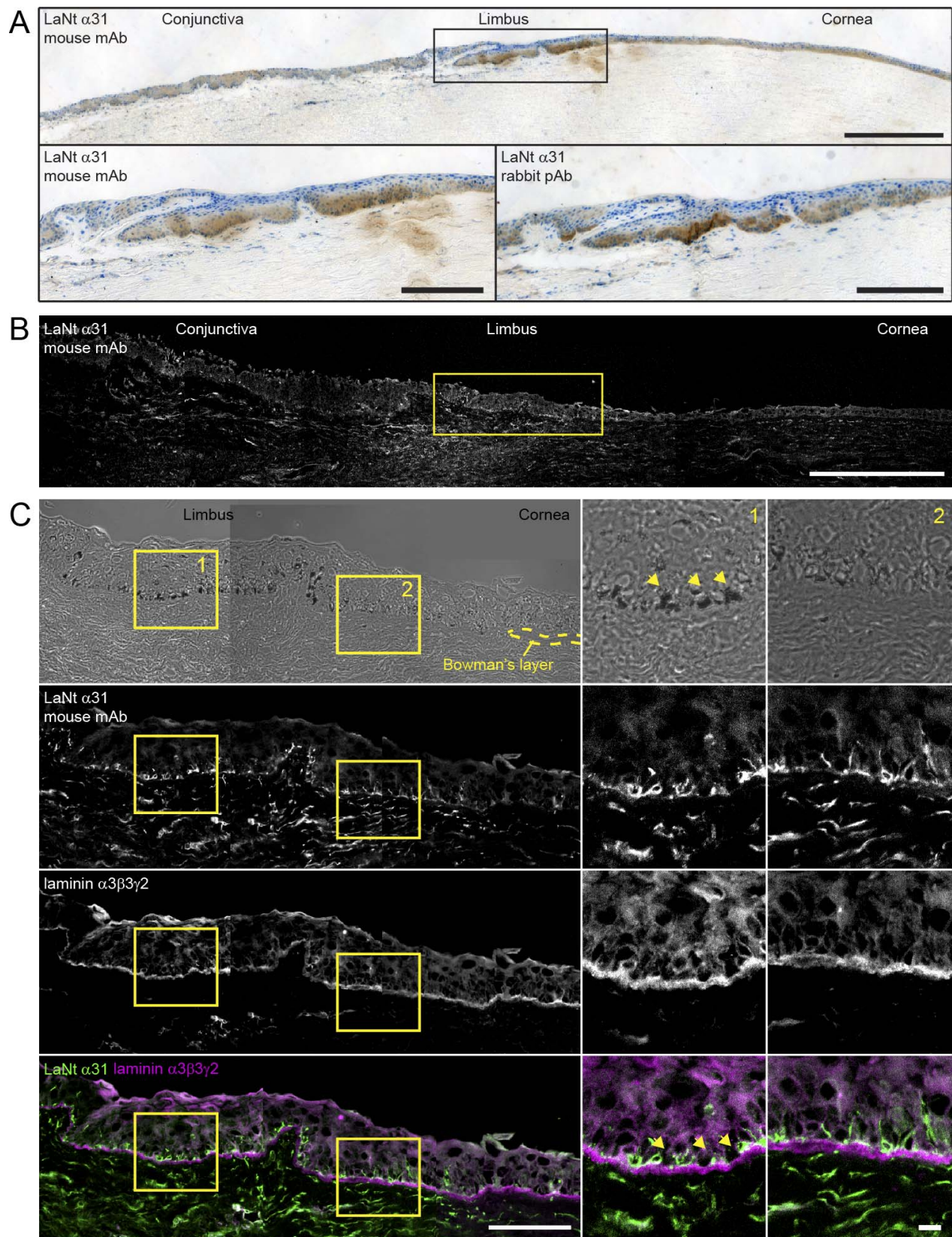
FIGURE 1. LaNt α31 protein is differentially distributed across ocular anterior segment epithelium. (**A**) Paraffin-embedded human anterior segment serial sections processed for immunohistochemistry with mouse monoclonal anti-LaNt α31 antibodies (*top* and *lower left*) or rabbit polyclonal anti-LaNt α31 (*lower right*). *Boxed region* at top shown at higher magnification in lower parts of figure. *Scale bars*: 500 μm (*top*); 200 μm (*lower*). (**B**, **C**) OCT-embedded human anterior segment section processed with mouse mAb antibodies against LaNt α31 and rabbit polyclonal antibodies against LM332. (**B**) Low-magnification stitched image of anterior surface epithelium; *scale bar*: 500 μm. *Yellow boxed region* shown at higher magnification in (**C**). (**C**) *Upper*: phase-contrast image; *yellow dotted line* denotes the end of Bowman's layer, the start of the corneal epithelium. *Second and third*

Investigative Ophthalmology & Visual Science

images: single channel image of LaNt α31 and LM332 antibody stains, respectively. *Bottom*: merged image with LaNt α31 pseudo-colored *green* and LM332 pseudo-colored *magenta*. *Scale bar*: 100 μm. *Boxed regions* 1 and 2 shown at higher magnification at right. *Yellow arrows* indicate location of limbal melanocytes. *Scale bar*: 10 μm.

display strong suprabasal staining in the peripheral cornea compared with 4/10 in conjunctiva; Supplementary Fig. S2; Supplementary Table S2). In addition to the epithelial layers, limbal vessels also displayed positive reactivity in most cases, consistent with reports of laminin α3b expression in blood vessels.[53]

In order to obtain higher-resolution distribution data and perform co-localization studies, we next processed frozen human anterior segments for indirect immunofluorescence microscopy with antibodies against LM332 along with mouse mAbs against anti-LaNt α31 (Figs. 1B, 1C) or with the rabbit anti-LaNt α31 pAb and mouse mAbs to laminin α3 (Supplementary Fig. S1C). Consistent with paraffin section staining, this revealed enrichment of LaNt α31 expression in the limbal epithelial regions relative to cornea. With fluorescence staining, stromal reactivity was much more pronounced than with immunohistochemistry, though both approaches displayed positivity in cells surrounding limbal vessels (Fig. 1B). In addition, the fluorescence images revealed occasional immunoreactivity of dendritic-like processes possibly associated with melanocytes. Closer examination of the limbal epithelium revealed subpopulations of reactivity, with enrichment along the basal aspect of epithelial cells apical to the strongest LM332 reactivity (Fig. 1C; Supplementary Fig. S1B). Interruptions in LaNt α31 staining frequently coincided with the location of melanocytes (Fig. 1C, arrowheads).

LaNt α31 Distribution in Ocular Surface Epithelium Is Conserved Between Mouse, Pig, and Human

Next, we compared LaNt α31 distribution between species. The rabbit pAb to human LaNt α31 was raised against a large region of the protein and therefore we predicted reactivity to the porcine version of the protein. Processing frozen and paraffin-embedded pig anterior segment sections with this antibody revealed a similar overall distribution pattern to that observed in human samples. Specifically, basal cells stained throughout all epithelium types, but local variation in terms of intensities and localization was observed; limbus and conjunctival regions were more strongly stained than the central cornea (Fig. 2). Indeed, the corneal epithelial staining was comparatively weak and more restricted in distribution to the matrix-associated aspect of basal cells, whereas more general cell staining was observed in limbal and conjunctival regions. Suprabasal reactivity was also present in conjunctiva and limbus and, also consistent with human samples, stromal structures including blood vessels displayed immunoreactivity (Fig. 2).

The specific peptide used to generate the mouse monoclonal antibody is not conserved between species (Supplementary Fig. S4A). Therefore, as a further negative control validation for the new mouse mAb, we processed porcine ocular surface sections and obtained equivalent signal intensity and distribution as obtained with isotype-matched IgG control treated sections (Supplementary Fig. S4B).

As an additional tool to investigate this new protein, and as further validation for these human and pig data, we raised rabbit polyclonal antibodies against a peptide unique to the mouse form of LaNt α31. As for human and pig sections, staining was observed throughout the ocular surface epithelium, with basal cell enrichment in conjunctival, limbus, and corneal epithelium; however, we again observed suprabasal reactivity, including small regions of the cornea where no distinct basal enrichment relative to suprabasal was observed (Supplementary Fig. S4C).

LaNt α31 Distribution in Limbal Subpopulations Mirrors K15, EGFR, and p63α

The variability in LaNt α31 staining intensities across the ocular surface and, specifically, the localized enrichment in basal epithelial cells of limbal regions suggested the possibility that this differential expression was indicative of subpopulations of cells. The limbal epithelium harbors stem cell niches and populations of transit-amplifying cells; we therefore next processed serial sections with antibodies against LaNt α31 and against K15, p63α, and EGFR (Fig. 3A).[54–60] Staining for each of these proteins was detected in clusters of cells in the basal regions of the limbus, and these clusters broadly correlated with regions where LaNt α31 staining was relatively enriched (Fig. 3A).

This potential correlation prompted us to next ask if the LaNt α31 expression changes during times when stem cells are active. To address this, we used an ex vivo stem cell activation model where human corneal–limbal rims obtained as surplus to requirements from corneal graft surgery were cultured for 14 days to stimulate LESC activation, as determined by presence of an epithelial outgrowth from the explant (Fig. 3B), before processing for immunohistochemistry and hematoxylin and eosin (H & E) staining (Fig. 3C).

In the explant sections, as expected, K15, p63α, and EGFR all displayed increased staining in the limbal epithelium and throughout the growing epithelial sheets, with definitive basal cell enrichment throughout the outgrowth (Fig. 3C). LaNt α31 staining was observed in near-identical patterns, with strong basal staining in the activated limbal cells and growing epithelium.

LaNt α31 Is Dynamically Redistributed During Corneal Wound Repair

Increased expression of LaNt α31 following introduction of a scratch wound in two-dimensional (2D) cultured epidermal keratinocytes has previously been described.[1] We therefore next wanted to determine what happens to LaNt α31 expression and distribution in a more physiologically relevant porcine ex vivo three-dimensional (3D) alkali wound model (Fig. 4A). Anterior segments were fixed at 24, 36, 48, or 72 hours after wounding, then processed for immunohistochemistry with rabbit anti-human LaNt antibodies (Figs. 4B–D). Strong LaNt α31 staining was observed across all layers of the epithelial cells surrounding the wound from 24 hours after wounding (Fig. 4B); however, staining intensity was reduced at 48 hours following wounding, by which point the wound was covered by nascent epithelium (Fig. 4B). In contrast, 72 hours following wounding, by which point the epithelium was more mature and more similar to unwounded tissue, LaNt α31 expression was again predominantly restricted to the basal layer (Fig. 4B), similar to what was observed in unwounded tissue.

Interestingly, in the limbal region, distinct populations of basal epithelial cells were highly enriched in LaNt α31 throughout the wound process (Fig. 4C). Strikingly, these populations of positive cells extended into the peripheral cornea during active repair; and in this region, those cells
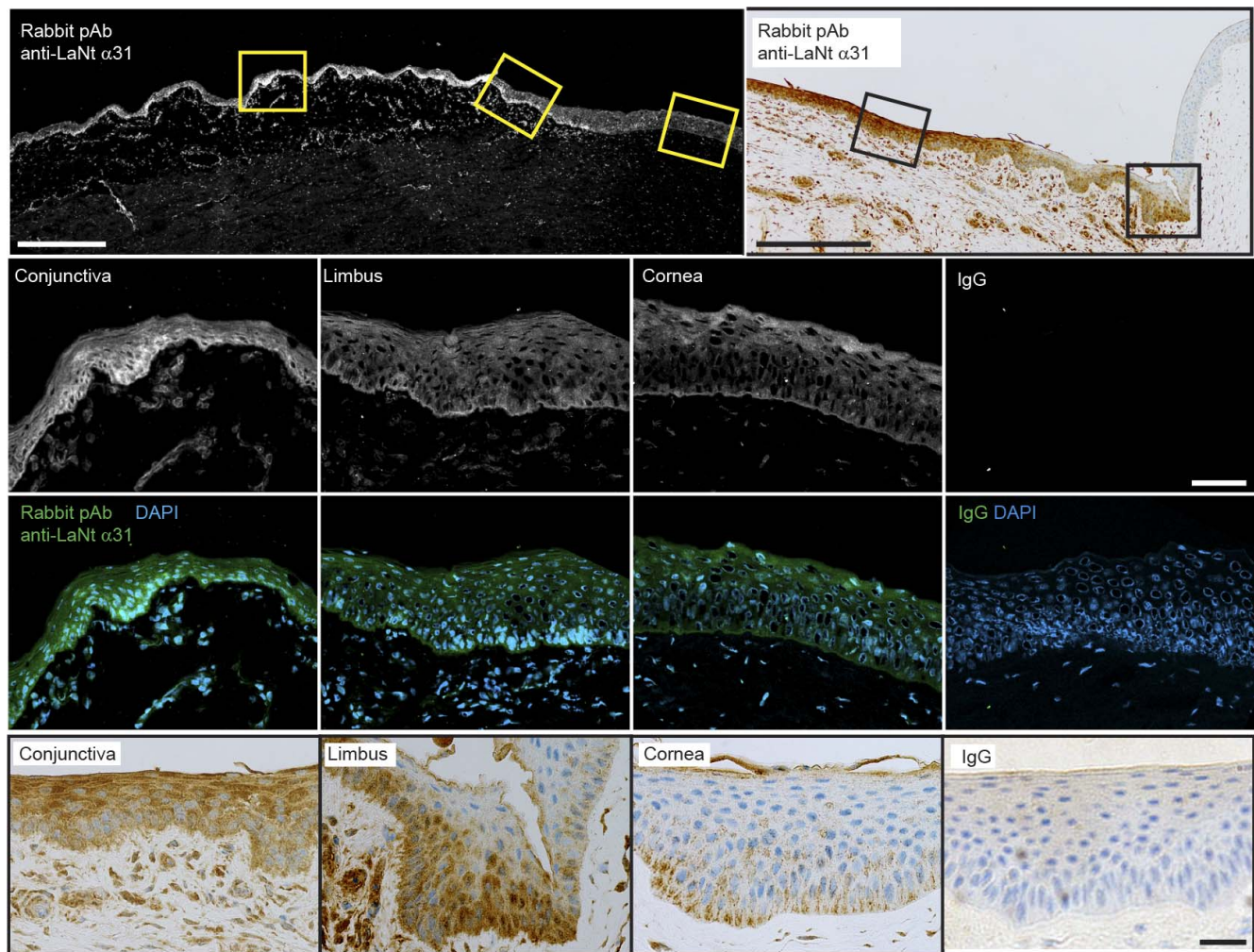
FIGURE 2. LaNt α31 displays lower expression in pig corneal epithelium than limbal and conjunctival epithelium. OCT (*top left* and *middle*) or paraffin-embedded (*top right* and *lower*) porcine anterior segments processed for indirect immunofluorescence microscopy or immunohisto-chemistry, respectively, with rabbit polyclonal antibodies against LaNtα31 or rabbit IgG (pseudo-colored *green* in merged images). Nuclei are counterstained with DAPI (pseudo-colored *blue* in merged) or hematoxylin. *Yellow boxed regions* in upper and *black boxed region* in lower left are shown at higher magnification below and to the right, respectively. *Scale bars*: 500 μm (*top*); 50 μm (*middle* and *lower*).

displaying high LaNt α31 expression appeared to display larger cross-sectional area compared with adjacent low-expressing basal cells (Fig. 4D). Together these data suggest a role for LaNt α31 in corneal repair and epithelial morphology and matura-tion.

Induced Expression of LaNt α31 in Limbal-Derived Epithelial Cells Leads to Increased Cell Spreading and Reduced Migration Rates

As our wound and stem cell models indicated transient and localized increases in LaNt α31 expression, we next investi-gated the impact that increased LaNt α31 levels have on cell behavior. To do so, we cultured pCEC from limbal explants and used an adenoviral delivery mechanism to induce LaNt α31 GFP expression (Supplementary Fig. S1B). Keratin 12 staining was used to validate the corneal epithelial lineage of isolated keratinocytes (Supplementary Fig. S5).

Consistent with the apparent increase in cell area in the peripheral cornea of pig wounds, the quantity of limbal-derived epithelial cells expressing LaNt α31 GFP 2D area was, on average, approximately twice that of GFP-expressing control cells and nontransduced pCEC (2D area + LaNt α31 $2720 \pm 720 \ \mu m^2$ versus pCEC $1230 \pm 380 \ \mu m^2$ and +GFP $1280 \pm 280 \ \mu m^2$, $P < 0.05$) (Figs. 5A, 5B). We next assessed single cell motility by plating the transduced cells at low density on uncoated dishes and then tracking motility over 2 hours (Fig. 5C). These analyses revealed the LaNt α31 GFP-expressing cells to display significantly reduced cell migration rates compared with controls (+LaNt α31 $0.46 \pm 0.14 \ \mu m/min$ versus pCEC $0.91 \pm 0.14 \ \mu m/min$ and +GFP $0.77 \pm 0.04 \ \mu m/$ min, mean values for all donors, $P < 0.05$) (Fig. 5D).

DISCUSSION

The data presented here demonstrate a differential distribution of LaNt α31 across the ocular surface epithelium that changes during corneal wound repair, and that largely mimics limbal epithelial stem/transit-amplifying cell–associated proteins in activated limbal explants. Moreover, in vitro data indicate that LaNt α31 can influence the adhesion and migration character-istics of limbal-derived corneal epithelial cells. These findings implicate LaNt α31 as a new, potentially important, player in corneal homeostasis and wound repair.
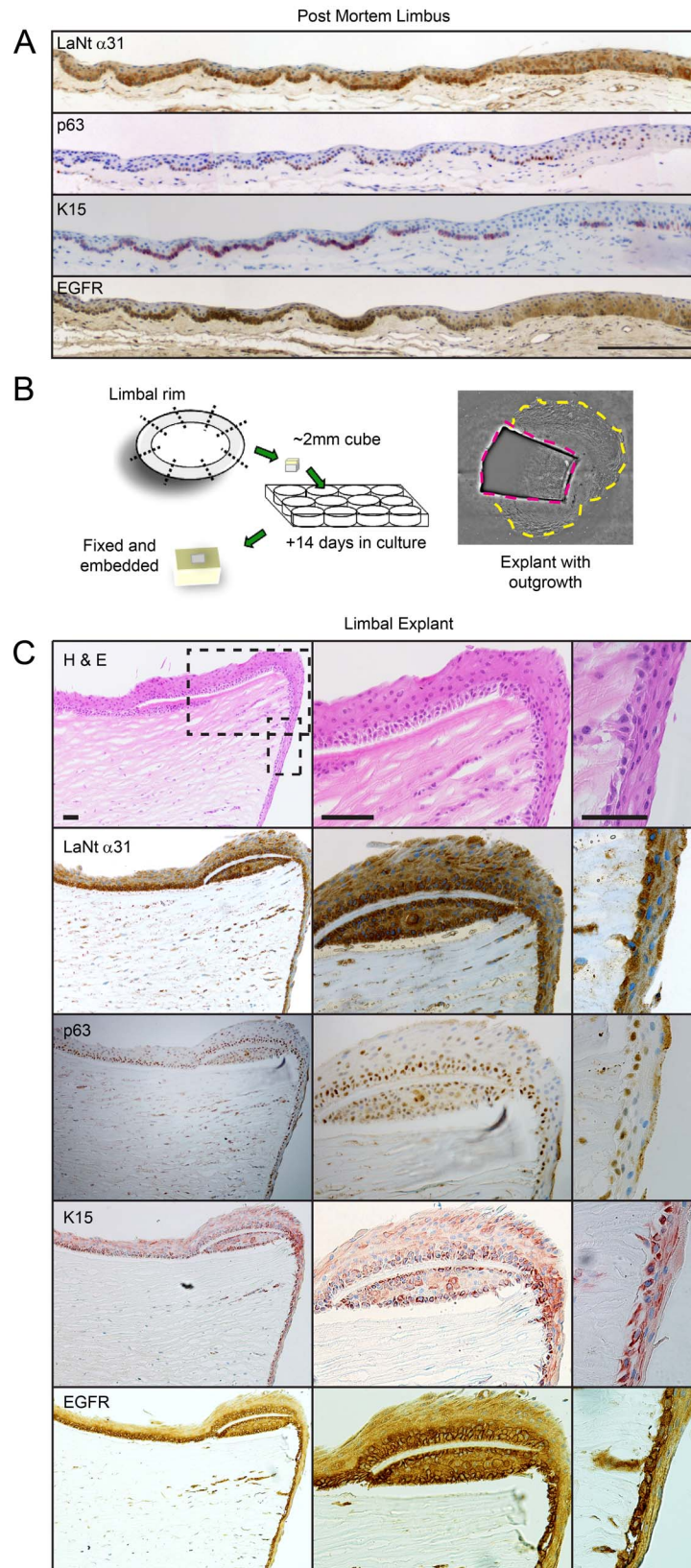
FIGURE 3. LaNt α31 is enriched in populations of cells positive for K15, EGFR, and p63α. (**A**) Serial sections from human anterior segments processed with antibodies against LaNt α31, or against p63α, K15, or EGFR. *Scale bar*: 200 μm. (**B**) Diagram of limbal explant culture system. *Inset*: phase-contrast image showing epithelial outgrowth following 14 days in culture. *Magenta dashed area* marks boundary of explant; *yellow dashed line* indicates outgrowth of epithelial cells. (**C**) Serial explant sections processed for H & E or with indicated antibodies against LaNt α31, p63α, K15, or EGFR. *Middle* and *right* in (**C**) show *dashed boxed* regions at higher magnification. *Scale bars*: 50 μm.
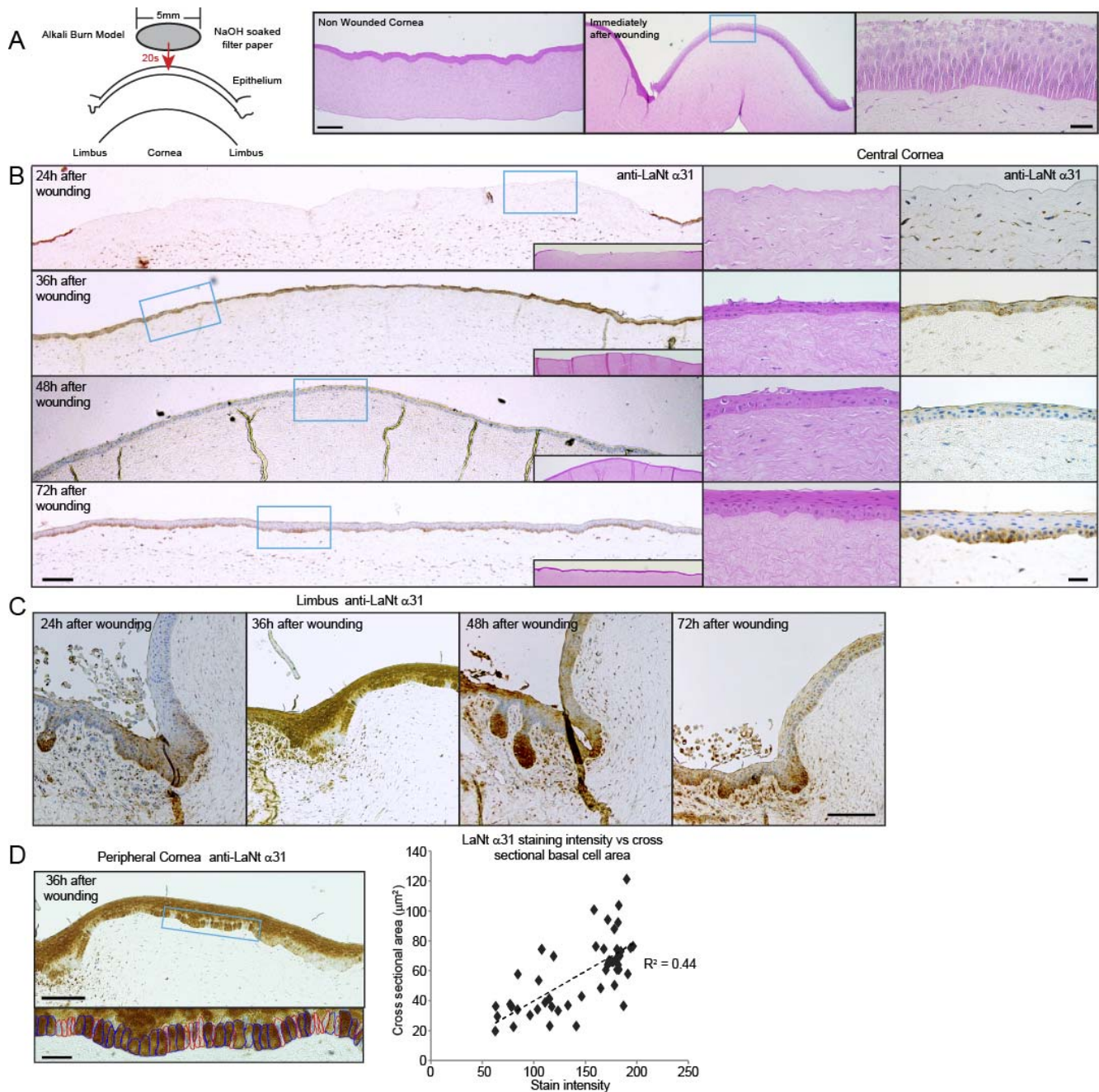
FIGURE 4. LaNt α31 is highly expressed during corneal wound healing. (A) Diagram of ex vivo wound healing model using porcine eyes. *Middle* in (A) shows wounded and unwounded porcine anterior segment sections processed for H & E staining; *right* shows a higher magnification of the damaged corneal epithelium (note lighter suprabasal staining indicating damage). (B–D) Paraffin sections at different time points from wounded porcine anterior segments processed with rabbit polyclonal antibodies raised against human LaNt α31 of the central cornea (B), limbus (C), and peripheral cornea (D). *Boxed regions* are shown at higher magnification to *right* in (B) along with serial sections processed for H & E. Cross-sectional area of basal epithelial cells was quantified by manually tracing cell borders in (D), then plotted against stain intensity. *Scale bars*: 100 μm (*left images* [A–C] and *top image* [D]); 20 μm (*right* [B] and *lower* [D]).

The best-supported model of corneal regeneration after injury involves cell proliferation in the limbus followed by migration from the limbus toward the cornea. Our finding that LaNt α31 is enriched in an activated limbus but reduced in an actively healing cornea, combined with corneal cell migration being slowed in the presence of high LaNt α31 levels, indicates that spatial and temporal control is required. Indeed, our induced expression data were somewhat surprising, as knockdown of LaNt α31 leads to reduced migration in HaCaT epidermal keratinocytes.[1] The primary corneal-like cells used here are slightly different from HaCaT, with higher baseline migration rates; however, together these data suggest that there is an optimum LaNt α31 concentration for migration, and moreover that titration of the LaNt α31 expression level could have evolved as means of switching corneal cells between a migratory, wound healing phenotype and an adherent mature epithelium.
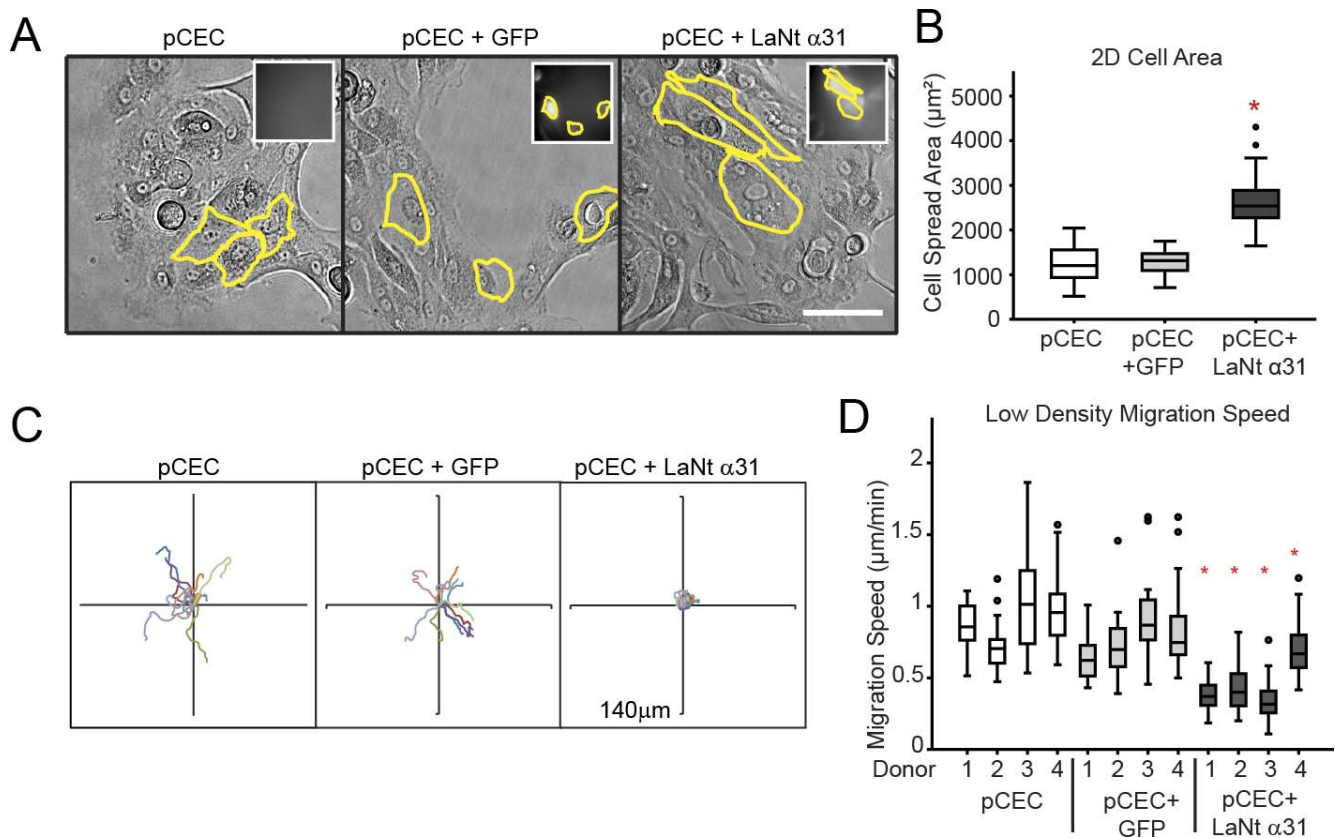
FIGURE 5. Increased LaNt α31 expression leads to increased cell area, decreased migration speed, and laminin organizational changes. (**A**) Primary corneal epithelial cells (pCEC) transduced with adenovirus encoding GFP (+GFP) or LaNt α31 GFP (+LaNt α31) were plated on uncoated plastic dishes, then imaged 16 hours later. *Inset* images show *green* fluorescent images; *yellow outlines* delineate cell borders of transduced cells. *Scale bar*: 50 μm. (**B**) 2D cell area generated from four donor explants with a minimum of 30 transduced cells per donor plotted as box and whisker plot. (**C**, **D**) pCECs were plated overnight on uncoated plastic coverslips and migration paths of individual cells tracked over a 2-hour period. (**C**) Representative tracks of 10 cells; each *colored line* represents path taken by an individual cell. (**D**) Total distance travelled over time (speed) of indicated cell treatments plotted as box and whisker plots from a minimum of 30 transduced cells per donor. *Boxes* in (**B**, **D**) represent 25th and 75th percentile, *whiskers* 5th and 95th percentile. *Red asterisks* denote $P < 0.05$ from both pCEC and +GFP cells as determined by 1-way ANOVA followed by Tukey's post hoc test.

The shared domains between LaNt α31 and laminins predict an ability to influence BM assembly via interaction with laminins influencing the latter's network assembly. Changes to laminin matrix organization could explain the observed influences on cell behavior. However, the LaNt α31 domain architecture also resembles that of the netrin proteins, which are best known as signaling proteins. While immunofluorescence imaging does suggest association with BM, the basal subpopulation enrichment of LaNt α31 is similar to that described for netrin-1 and netrin-4,[42,61] although it is striking to note that in the mouse eye, netrin-4 has been shown to be highly expressed in the cornea but not in the limbal regions of the developing or adult eye—effectively the mirror image to LaNt α31.[62] Netrin-4 has also been established as capable of influencing laminin interactions both in vitro and in vivo,[39,40] and, as such, LaNt α31 may turn out to be a new class of laminin-derived netrins.

As one would expect from a study of a "new" protein, these findings have generated additional questions. One of the surprising findings of our study was the presence of the LaNt α31 protein in layers above the basal layer, as we would predict a protein derived from a laminin gene to be located only in BM-associated regions. This staining was observed in mouse, human, and pig sections, using three different antibody preparations, and, as such, we do not believe it to be a

processing artifact. The finding of LaNt α31 expression in suprabasal cells raises questions of whether the protein continues to be translated from long-lived mRNAs, or if we are detecting protein that has been retained within the cells as they differentiate, or whether the transcript continues to be produced. What role, if any, LaNt α31 plays in the suprabasal cells will be an interesting future direction.

We also observed antibody reactivity in limbal and conjunctival stromal regions in all three species. These findings are less surprising, as the promoter that drives LaNt α31 production has been shown to be active in NIH3T3 fibroblasts,[20] and laminin α3b protein has also been described as being expressed in the dermal microvasculature.[53] What roles the LaNt α31 plays in these contexts is as yet unknown; however mesenchymal cells, including fibroblasts and pericytes, contribute to BM formation, and therefore the simplest explanation is that the LaNt protein from the limbal stroma is ultimately involved in establishing the epithelial BM.

Maintenance and effective repair of the ocular surface epithelium is essential to preserve vision and relies on precise regulation of a number of overlapping cellular functions. including proliferation and differentiation, adhesion and migration, and extracellular matrix remodeling. Together, the data presented here implicate the LaNt α31 protein as a player in numerous aspects of these processes. Ultimately this may be

relevant not only for wound repair but also in conditions such as recurrent corneal erosions where defective BM and cell to matrix–adhesion reassembly are associated with loss of corneal epithelial integrity.[6,27,28]

References

1. Hamill KJ, Langbein L, Jones JC, McLean WH. Identification of a novel family of laminin N-terminal alternate splice isoforms: structural and functional characterization. *J Biol Chem*. 2009; 284:35588–35596.

2. Bystrom B, Virtanen I, Rousselle P, Gullberg D, Pedrosa-Domellof F. Distribution of laminins in the developing human eye. *Invest Ophthalmol Vis Sci*. 2006;47:777–785.

3. Kabosova A, Azar DT, Bannikov GA, et al. Compositional differences between infant and adult human corneal basement membranes. *Invest Ophthalmol Vis Sci*. 2007;48:4989–4999.

4. Ljubimov AV, Burgeson RE, Butkowski RJ, et al. Basement membrane abnormalities in human eyes with diabetic retinopathy. *J Histochem Cytochem*. 1996;44:1469–1479.

5. Ljubimov AV, Burgeson RE, Butkowski RJ, Michael AF, Sun TT, Kenney MC. Human corneal basement membrane heterogeneity: topographical differences in the expression of type IV collagen and laminin isoforms. *Lab Invest*. 1995;72:461–473.

6. Pal-Ghosh S, Pajoohesh-Ganji A, Tadvalkar G, Stepp MA. Removal of the basement membrane enhances corneal wound healing. *Exp Eye Res*. 2011;93:927–936.

7. Schlotzer-Schrehardt U, Dietrich T, Saito K, et al. Characterization of extracellular matrix components in the limbal epithelial stem cell compartment. *Exp Eye Res*. 2007;85:845–860.

8. Hamill KJ, Kligys K, Hopkinson SB, Jones JC. Laminin deposition in the extracellular matrix: a complex picture emerges. *J Cell Sci*. 2009;122:4409–4417.

9. Aumailley M. The laminin family. *Cell Adh Migr*. 2013;7:48–55.

10. Hohenester E, Yurchenco PD. Laminins in basement membrane assembly. *Cell Adh Migr*. 2013;7:56–63.

11. Radisky DC. Function following form: functional differentiation of mammary epithelial cells requires laminin-induced polarization of PI3-kinase. *Cell Cycle*. 2011;10:15.

12. Kikkawa Y, Kataoka A, Matsuda Y, et al. Maintenance of hepatic differentiation by hepatocyte attachment peptides derived from laminin chains. *J Biomed Mater Res A*. 2011;99:203–210.

13. Akerlund M, Carmignac V, Scheele S, Durbeej M. Laminin alpha1 domains LG4-5 are essential for the complete differentiation of visceral endoderm. *Cell Tissue Res*. 2009;338:129–137.

14. van Dijk A, Niessen HW, Zandieh Doulabi B, Visser FC, van Milligen FJ. Differentiation of human adipose-derived stem cells towards cardiomyocytes is facilitated by laminin. *Cell Tissue Res*. 2008;334:457–467.

15. Hashimoto J, Ogawa T, Tsubota Y, Miyazaki K. Laminin-5 suppresses chondrogenic differentiation of murine teratocarcinoma cell line ATDC5. *Exp Cell Res*. 2005;310:256–269.

16. Chen ZL, Strickland S. Laminin gamma1 is critical for Schwann cell differentiation, axon myelination, and regeneration in the peripheral nerve. *J Cell Biol*. 2003;163:889–899.

17. Okumura N, Kakutani K, Numata R, et al. Laminin-511 and -521 enable efficient in vitro expansion of human corneal endothelial cells. *Invest Ophthalmol Vis Sci*. 2015;56:2933–2942.

18. Polisetti N, Sorokin L, Okumura N, et al. Laminin-511 and -521-based matrices for efficient ex vivo-expansion of human limbal epithelial progenitor cells. *Sci Rep*. 2017;7:5152.

19. Ryan MC, Tizard R, VanDevanter DR, Carter WG. Cloning of the LamA3 gene encoding the alpha 3 chain of the adhesive ligand epiligrin. Expression in wound repair. *J Biol Chem*. 1994;269:22779–22787.

20. Ferrigno O, Virolle T, Galliano MF, et al. Murine laminin alpha3A and alpha3B isoform chains are generated by usage of two promoters and alternative splicing. *J Biol Chem*. 1997; 272:20502–20507.

21. Figueira EC, Murrell DF, Coroneo MT. Ophthalmic involvement in inherited epidermolysis bullosa. *Dermatol Clin*. 2010;28:143–152.

22. Hammerton ME, Turner TW, Pyne RJ. A case of junctional epidermolysis bullosa (Herlitz-Pearson) with corneal bullae. *Aust J Ophthalmol*. 1984;12:45–48.

23. Kirtschig G, Marinkovich MP, Burgeson RE, Yancey KB. Anti-basement membrane autoantibodies in patients with anti-epiligrin cicatricial pemphigoid bind the alpha subunit of laminin 5. *J Invest Dermatol*. 1995;105:543–548.

24. Lazarova Z, Yee C, Lazar J, Yancey KB. IgG autoantibodies in patients with anti-epiligrin cicatricial pemphigoid recognize the G domain of the laminin 5 alpha-subunit. *Clin Immunol*. 2001;101:100–105.

25. Fukuchi O, Suko A, Matsuzaki H, et al. Anti-laminin-332 mucous membrane pemphigoid with autoantibodies to alpha3, beta3 and gamma2 subunits of laminin-332 as well as to BP230 and periplakin associated with adenocarcinoma from an unknown primary site. *J Dermatol*. 2013;40:61–62.

26. McLean WH, Irvine AD, Hamill KJ, et al. An unusual N-terminal deletion of the laminin alpha3a isoform leads to the chronic granulation tissue disorder laryngo-onycho-cutaneous syndrome. *Hum Mol Genet*. 2003;12:2395–2409.

27. Oliver VF, van Bysterveldt KA, Cadzow M, et al. A COL17A1 splice-altering mutation is prevalent in inherited recurrent corneal erosions. *Ophthalmology*. 2016;123:23.

28. Pal-Ghosh S, Blanco T, Tadvalkar G, et al. MMP9 cleavage of the beta4 integrin ectodomain leads to recurrent epithelial erosions in mice. *J Cell Sci*. 2011;124:2666–2675.

29. Ebihara N, Watanabe Y, Nakayasu K, Kanai A. The expression of laminin-5 and ultrastructure of the interface between basal cells and underlying stroma in the keratoconus cornea. *Jpn J Ophthalmol*. 2001;45:209–215.

30. Kenney MC, Nesburn AB, Burgeson RE, Butkowski RJ, Ljubimov AV. Abnormalities of the extracellular matrix in keratoconus corneas. *Cornea*. 1997;16:345–351.

31. Nielsen PK, Gho YS, Hoffman MP, et al. Identification of a major heparin and cell binding site in the LG4 module of the laminin alpha 5 chain. *J Biol Chem*. 2000;275:14517–14523.

32. Timpl R, Tisi D, Talts JF, Andac Z, Sasaki T, Hohenester E. Structure and function of laminin LG modules. *Matrix Biol*. 2000;19:309–317.

Investigative Ophthalmology & Visual Science

33. Shang M, Koshikawa N, Schenk S, Quaranta V. The LG3 module of laminin-5 harbors a binding site for integrin alpha3beta1 that promotes cell adhesion, spreading, and migration. *J Biol Chem*. 2001;276:33045–33053.

34. Kadoya Y, Mochizuki M, Nomizu M, Sorokin L, Yamashina S. Role for laminin-alpha5 chain LG4 module in epithelial branching morphogenesis. *Dev Biol*. 2003;263:153–164.

35. Okamoto O, Bachy S, Odenthal U, et al. Normal human keratinocytes bind to the alpha3LG4/5 domain of unprocessed laminin-5 through the receptor syndecan-1. *J Biol Chem*. 2003;278:44168–44177.

36. Cheng YS, Champliaud MF, Burgeson RE, Marinkovich MP, Yurchenco PD. Self-assembly of laminin isoforms. *J Biol Chem*. 1997;272:31525–31532.

37. Yurchenco PD, Cheng YS. Self-assembly and calcium-binding sites in laminin. A three-arm interaction model. *J Biol Chem*. 1993;268:17286–17299.

38. Yurchenco PD, Tsilibary EC, Charonis AS, Furthmayr H. Laminin polymerization in vitro. Evidence for a two-step assembly with domain specificity. *J Biol Chem*. 1985;260:7636–7644.

39. Schneiders FI, Maertens B, Bose K, et al. Binding of netrin-4 to laminin short arms regulates basement membrane assembly. *J Biol Chem*. 2007;282:23750–23758.

40. Reuten R, Patel TR, McDougall M, et al. Structural decoding of netrin-4 reveals a regulatory function towards mature basement membranes. *Nat Commun*. 2016;7:13515.

41. Maier AB, Klein S, Kociok N, et al. Netrin-4 mediates corneal hemangiogenesis but hot lymphangiogenesis in the mouse-model of suture-induced neovascularization. *Invest Ophthalmol Vis Sci*. 2017;58:1387–1396.

42. Han Y, Shao Y, Liu T, Qu YL, Li W, Liu Z. Therapeutic effects of topical netrin-4 inhibits corneal neovascularization in alkali-burn rats. *PLoS One*. 2015;10:e0122951.

43. Han Y, Shao Y, Lin Z, et al. Netrin-1 simultaneously suppresses corneal inflammation and neovascularization. *Invest Ophthalmol Vis Sci*. 2012;53:1285–1295.

44. Li YN, Pinzon-Duarte G, Dattilo M, Claudepierre T, Koch M, Brunken WJ. The expression and function of netrin-4 in murine ocular tissues. *Exp Eye Res*. 2012;96:24–35.

45. Torricelli AA, Singh V, Santhiago MR, Wilson SE. The corneal epithelial basement membrane: structure, function, and disease. *Invest Ophthalmol Vis Sci*. 2013;54:6390–6400.

46. Kurpakus MA, Stock EL, Jones JC. Expression of the 55-kD/64-kD corneal keratins in ocular surface epithelium. *Invest Ophthalmol Vis Sci*. 1990;31:448–456.

47. Langhofer M, Hopkinson SB, Jones JC. The matrix secreted by 804G cells contains laminin-related components that participate in hemidesmosome assembly in vitro. *J Cell Sci*. 1993;105(pt 3):753–764.

48. Gonzales M, Haan K, Baker SE, et al. A cell signal pathway involving laminin-5, alpha3beta1 integrin, and mitogen-activated protein kinase can regulate epithelial cell proliferation. *Mol Biol Cell*. 1999;10:259–270.

49. Galfre G, Milstein C. Preparation of monoclonal antibodies: strategies and procedures. *Methods Enzymol*. 1981;73:3–46.

50. Boukamp P, Stanbridge EJ, Foo DY, Cerutti PA, Fusenig NE. c-Ha-ras oncogene expression in immortalized human keratinocytes (HaCaT) alters growth potential in vivo but lacks correlation with malignancy. *Cancer Res*. 1990;50:2840–2847.

51. Anderson C, Zhou Q, Wang S. An alkali-burn injury model of corneal neovascularization in the mouse. *J Vis Exp*. 2014;86

52. Boukamp P, Petrussevska RT, Breitkreutz D, Hornung J, Markham A, Fusenig NE. Normal keratinization in a spontaneously immortalized aneuploid human keratinocyte cell line. *J Cell Biol*. 1988;106:761–771.

53. Kariya Y, Mori T, Yasuda C, et al. Localization of laminin alpha3B chain in vascular and epithelial basement membranes of normal human tissues and its down-regulation in skin cancers. *J Mol Histol*. 2008;39:435–446.

54. Yoshida S, Shimmura S, Kawakita T, et al. Cytokeratin 15 can be used to identify the limbal phenotype in normal and diseased ocular surfaces. *Invest Ophthalmol Vis Sci*. 2006;47:4780–4786.

55. Morita S, Shirakata Y, Shiraishi A, et al. Human corneal epithelial cell proliferation by epiregulin and its cross-induction by other EGF family members. *Mol Vis*. 2007;13:2119–2128.

56. Chen Z, de Paiva CS, Luo L, Kretzer FL, Pflugfelder SC, Li DQ. Characterization of putative stem cell phenotype in human limbal epithelia. *Stem Cells*. 2004;22:355–366.

57. Zieske JD, Takahashi H, Hutcheon AE, Dalbone AC. Activation of epidermal growth factor receptor during corneal epithelial migration. *Invest Ophthalmol Vis Sci*. 2000;41:1346–1355.

58. Kalha S, Shrestha B, Sanz Navarro M, Jones KB, Klein OD, Michon F. Bmi1+ progenitor cell dynamics in murine cornea during homeostasis and wound healing. *Stem Cells*. 2018;36:562–573.

59. Levis HJ, Daniels JT. Recreating the human limbal epithelial stem cell niche with bioengineered limbal crypts. *Curr Eye Res*. 2016;41:1153–1160.

60. Stasi K, Goings D, Huang J, et al. Optimal isolation and xeno-free culture conditions for limbal stem cell function. *Invest Ophthalmol Vis Sci*. 2014;55:375–386.

61. Han Y, Shao Y, Lin Z, et al. Netrin-1 simultaneously suppresses corneal inflammation and neovascularization. *Invest Ophthalmol Vis Sci*. 2012;53:1285–1295.

62. Li YN, Pinzon-Duarte G, Dattilo M, Claudepierre T, Koch M, Brunken WJ. The expression and function of netrin-4 in murine ocular tissues. *Exp Eye Res*. 2012;96:24–35.